Preprints of the 21st IFAC World Congress (Virtual)
Berlin, Germany, July 12-17, 2020

Field Oriented Economic Model Predictive Control for Permanent Magnet Synchronous Motors ⋆

D. Geweth * **A. Zanelli** ** **G. Frison** ** **U. Vollmer** * **M. Diehl** **

* *Department of Automotive Electronic, Robert Bosch GmbH, 71701 Schwieberdingen, Germany, (e-mail: {daniel.geweth, ulrich.vollmer}@de.bosch.com).*
** *Department of Microsystems Engineering (IMTEK) and Department of Mathematics, University Freiburg, 79110 Freiburg, Germany (e-mail: {andrea.zanelli, gianluca.frison, moritz.diehl}@imtek.uni-freiburg.de)*

Abstract: This paper proposes a novel nonlinear model predictive control approach for permanent magnet synchronous machines (PMSM). The optimization problem is formulated as a field oriented economic model predictive control (FO-EMPC) problem and therefore a target selector is not necessary. A *dq*-model of the PMSM with spherical voltage and current constraints is taken into account. A terminal set and a terminal penalty are introduced to mitigate stability and convergence issues with a short prediction horizon. The performance of the proposed control scheme is demonstrated in a simulation study on a personal computer and in a hardware-in-the-loop simulation, which show that the transition time is reduced by more than one order of magnitude with respect to state-of-the-art approaches, especially when the voltage constraint becomes active.

Keywords: predictive control, electric motors, nonlinear systems

1. INTRODUCTION

Electrification is one of the major trends in the automotive sector. Therefore, electric drives play an increasingly important role within this industry. Due to their favourable properties such as compact size and good efficiency, three-phase permanent magnet synchronous machines (PMSM) are widely used in various applications such as electric or hybrid powertrains, but also electric power steering and other actuators. High-performance torque control of PMSMs is essential for these applications. Torque control usually consists of two distinct parts: The first part is the calculation of *dq*-current references from the torque reference. The second part is the feedback-control of currents. Standard electric drives do not contain a torque sensor, therefore the first part is carried out in open-loop, relying on offline optimization, which ensures that the desired torque is produced with minimum phase current amplitude (Schröder, 2015). For the second part, the state-of-the-art solution is classical field oriented control (CFOC), which has been developed in the early 1970s and has since then become standard in control of electric drives (Schröder, 2015). It ensures high control performance with moderate computational effort and it has a well-founded theory. However, the handling of voltage constraints is not straightforward and mainly based on heuristics, (Quang and Dittrich, 2008).

⋆ This research was supported by the German Federal Ministry for Economic Affairs and Energy (BMWi) via eco4wind (0324125B) and DyConPV (0324166B), and by DFG via Research Unit FOR 2401.

Model predictive control (MPC) is an optimization based approach in which constraints are inherently considered and handled explicitly. MPC has become popular since 1970 in the chemical process industry as a higher level control concept with underlying linear controllers, e.g. PID controllers. Recent advances in embedded computer technology and in the field of real-time optimization, (Kouzoupis et al., 2018), (Findeisen et al., 2018) and (Diehl et al., 2005), have reduced the computation time of MPC algorithms such that their application to control electric machines has become feasible, see (Englert and Graichen, 2018), (Riar et al., 2015) and (Zanelli et al., 2019). Two fundamentally different MPC approaches have been investigated for the current control of electric machines: MPC with a finite control set, see (Riar et al., 2015) and with a continuous control set, see (Englert and Graichen, 2018) and (Kisner and Konigorski, 2018). MPC with a continuous control set is typically based on a field oriented approach (FO-MPC) and the optimization problem can be formulated as a nonlinear program (NLP), which is typically solved with derivative based algorithms such as a sequential quadratic programming (SQP) scheme, see (Findeisen et al., 2018), (Graber, 2018) and (Diehl et al., 2005).

In this paper, a field oriented economic model predictive control (FO-EMPC) is proposed in which both parts of torque control mentioned above are integrated in a single one. The control problem is *not* split into a target selector and a phase current controller, but the torque control

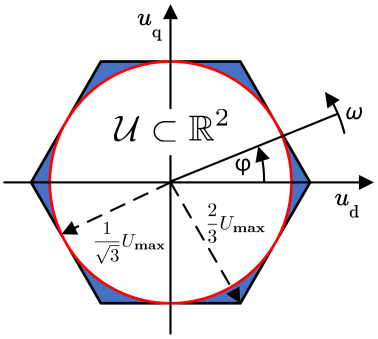

Fig. 1. The rotating hexagon voltage constraint with angular velocity ω and the approximating inner circle in the *dq*-coordinate system. The blue corners are not covered by the inner circle.

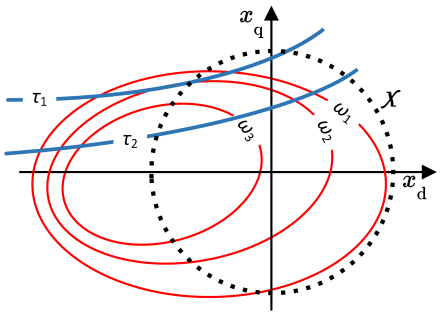

Fig. 2. The red ellipses show the region of feasible steady states depending on the speed. The iso-torque lines on two different levels are depicted in blue. The current constraint is represented by the black dotted circle.

problem is solved directly. This approach allows for a compact and flexible formulation by explicitly considering the torque equation in the optimization problem. A direct MPC approach with continuous control set is chosen which is solved in simulation on a personal computer using the software package `CasADi` (Andersson et al., 2018) with an interior point method. For the hardware in the loop (HIL) simulation a sequential convex quadratic programming (SCQP) is used, which is included in the software package `acados` (Verschueren et al., 2019).

The paper is organized as follows. In Section 2 the model of the electric machine, the constraints and a state-of-the-art CFOC are presented. Section 3 introduces the new FO-EMPC design and shows this approach to mitigate stability and convergence issues which occur when using a short prediction horizon. In Section 4, simulation results are presented and the control performance of FO-EMPC is compared with CFOC. Finally, a hardware-in-the-loop (HIL) simulation on dSPACE using the software package `acados` is discussed. A brief summary and outlook is given in Section 5.

2. MODEL AND CONSTRAINTS

This section presents the dynamical model of a PMSM and the constraints that have to be taken into account by the controller.

2.1 Electrical subsystem

The most common mathematical description of a PMSM is based on an ordinary differential equation (ODE) with the parameters $\varphi(t)$ and $\omega(t)$, where $\varphi(t)$ is the electrical rotor angle and $\omega(t)$ describes the electrical rotor speed. This formulation is named *abc*-model, due to the common notation of the line currents $i_l(t)$, with $l \in \{a, b, c\}$, and respectively the line voltages $u_l(t)$, with $l \in \{a, b, c\}$, with respect to ground. The ODE is nonlinear with respect to the parameter $\varphi(t)$, but linear in the line currents, line voltages and speed. The nonlinear description can be transformed with a diffeomorphism into an affine linear ODE without parameter φ. The diffeomorphism $T(\varphi(t)) : \mathbb{R}^3 \to \mathbb{R}^2$ is named *dq*-transformation. This method is well known, (Schröder, 2015; Quang and Dittrich, 2008), and is considered throughout the paper. With this transformation, the following model of the PMSM is obtained:

$$\dot{\mathbf{x}} = \mathbf{A}(\omega)\mathbf{x} + \mathbf{B}\mathbf{u} + \mathbf{f}(\omega), \quad \text{with} \tag{1}$$

$$\mathbf{A} = \begin{bmatrix} -\frac{R}{L_\mathrm{d}} & \frac{L_\mathrm{q}}{L_\mathrm{d}}\omega \\ -\frac{L_\mathrm{d}}{L_\mathrm{q}}\omega & -\frac{R}{L_\mathrm{q}} \end{bmatrix}, \mathbf{B} = \begin{bmatrix} \frac{1}{L_\mathrm{d}} & 0 \\ 0 & \frac{1}{L_\mathrm{q}} \end{bmatrix}, \mathbf{f} = \begin{bmatrix} 0 \\ -\frac{\omega\psi_\mathrm{pm}}{L_\mathrm{q}} \end{bmatrix},$$

and with the associated nonlinear torque equation

$$\tau(\mathbf{x}) = \frac{3}{2}N_\mathrm{p}((L_\mathrm{d} - L_\mathrm{p})x_\mathrm{d}x_\mathrm{q} + \psi_\mathrm{pm}x_\mathrm{q}). \tag{2}$$

Here $\mathbf{x} = (x_\mathrm{d}\ x_\mathrm{q})^\top$ is the state vector (current vector), $\mathbf{u} = (u_\mathrm{d}\ u_\mathrm{q})^\top$ is the input vector (voltage vector). The parameter ψ_pm is the permanent magnet flux linkage, N_p is the number of pole pairs, L_d and L_q are the *dq*-inductances and R the resistance. The motor parameters are shown in Table 1. Nonlinear effects such as magnetic saturation and iron losses are neglected. The back electromotive force (BEMF) is defined as:

$$L_\mathrm{d}\dot{x}_\mathrm{d} + Rx_\mathrm{d} = u_\mathrm{d} + \underbrace{L_\mathrm{q}\omega x_\mathrm{q}}_{u_\mathrm{d,BEMF}}, \tag{3a}$$

$$L_\mathrm{q}\dot{x}_\mathrm{q} + Rx_\mathrm{q} = u_\mathrm{q} - \underbrace{(L_\mathrm{d}x_\mathrm{d} + \psi_\mathrm{pm})\omega}_{u_\mathrm{q,BEMF}}. \tag{3b}$$

The BEMF, which depends on the states $\mathbf{x}$ and the speed ω, acts against the control voltage $\mathbf{u}$.

2.2 Constraints

Typical constraints in PMSM control are the current and voltage constraints and can be formulated as box constraints in the *abc*-system. Hence, through the *dq*-transformation, the box constraints are transformed into a hexagonal constraints, which depends on the angle $\varphi(t)$ and rotates with the electrical rotor speed ω. Figure 1 shows the resulting voltage constraints in *dq*-coordinates. In this paper the hexagon is approximated by an inner circle and the associated set is defined as:

$$\mathcal{U} := \left\{ (u_\mathrm{d}, u_\mathrm{q}) : u_\mathrm{d}^2 + u_\mathrm{q}^2 \leq \frac{1}{3}U_\mathrm{max}^2 \right\}. \tag{4}$$

Likewise, the set for the current is defined as

$$\mathcal{X} := \left\{ (x_\mathrm{d}, x_\mathrm{q}) : x_\mathrm{d}^2 + x_\mathrm{q}^2 \leq X_\mathrm{max}^2 \right\}. \tag{5}$$

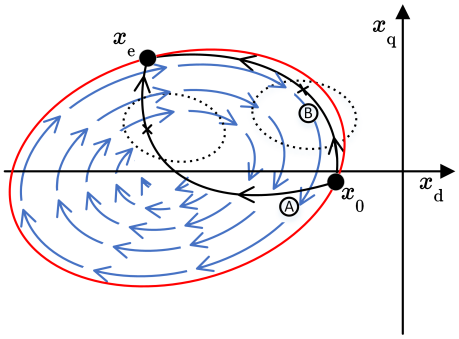

Fig. 3. Two different trajectories from starting point $\mathbf{x}_0$ to the endpoint $\mathbf{x}_e$ are pictured as black solid lines. The dotted ellipses around the intermediate states (black crosses) show the regions which are reachable in one time step. The blue arrows indicate the behaviour of the autonomous system caused by the BEMF and the ohmic voltage drop.

Due to the voltage constraint, the set of steady states is restricted, too. In fact, due to Equations (1) and (4), the feasible steady states are bounded by an ellipse, which depends on the speed ω:

$$(\mathbf{B}^{-1}(\mathbf{A}\mathbf{x}+\mathbf{f}))^T(\mathbf{B}^{-1}(\mathbf{A}\mathbf{x}+\mathbf{f})) \leq \frac{1}{3}U_{\max}^2. \quad (6)$$

The presented properties of the PMSM are summarized in Figure 2. Regardless of the current constraint, the interior of the red ellipses shows the reachable steady states at various speed values ω. The iso-torque lines (2) on different levels $\tau(\mathbf{x})$ are depicted in blue. It is shown that the set of all achievable steady states are decreasing with increasing speed and, consequently, a lower torque is reachable. The current constraint (5) is represented as a black dotted circle around the origin.

2.3 System analysis

This section analyses the system with main focus on transition time. The considered dq-model has a two dimensional control input $\mathbf{u} \in \mathbb{R}^2$, which generally allows to influence transition time and the direction of the trajectory (loosely speaking the eigenvalues and the eigenvectors of the autonomous system) (Konigorski, 2011). The relationship between transition time and direction is shown below. The autonomous system $\mathbf{u} = \mathbf{0}$ is not a conservative field, i.e.

$$\nabla \times \dot{\mathbf{x}}\big|_{\mathbf{u}=\mathbf{0}} \neq 0. \quad (7)$$

Therefore, with the controlled constrained system, with $\mathbf{u} \in \mathcal{U}$, the transition time from starting point $\mathbf{x}_0$ to the endpoint $\mathbf{x}_e$ depends on the chosen trajectory and, in turn, the control sequence $\mathbf{u}(t)$.

In Figure 3, two different trajectories are shown. Trajectory A goes through the interior of the ellipse and reaches the endpoint at time T_A. Trajectory B goes along the boundaries of the ellipse and takes T_B with $T_B > T_A$. The dotted ellipses around the intermediate states (black crosses) show each a region, which is reachable in one time step T_s. Hence on trajectory B, only a small advance per time unit in direction to $\mathbf{x}_e$ is possible. The result is caused by the BEMF, which is introduced in Section 2.1. The blue arrows in Figure 3 indicate the behaviour of the autonomous system caused by the BEMF and the Ohmic voltage drop.

Table 1. Parameters of the PMSM

Parameter	Value	Unit
R	$18.15 \cdot 10^{-3}$	Ω
L_d	$107 \cdot 10^{-6}$	H
L_q	$150 \cdot 10^{-6}$	H
ψ_pm	$13.8 \cdot 10^{-3}$	Vs
N_p	5	-
U_max	48	V
X_max	155	A
ω_max	4000	s^{-1}

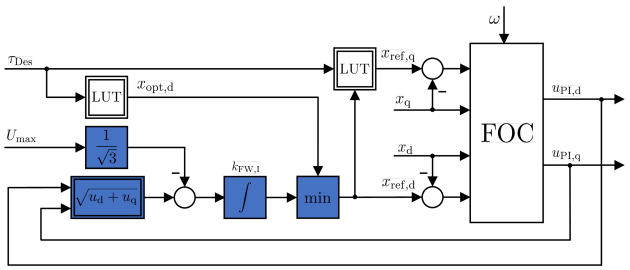

Fig. 4. FOC with an overlaying field weakening controller in blue. The first lookup table (LUT) includes the MTPA function. The second LUT describes the allocation from current in d-direction and desired torque to the current in q-direction.

2.4 Current reference calculation

In state-of-the-art PMSM control the current references are calculated offline. The optimal set points $x_{\mathrm{ref},l}, l \in \{\mathrm{d},\mathrm{q}\}$ with minimized copper losses for the unconstrained system are given by the maximum torque per ampere (MTPA) function, (see (Schröder, 2015)), which is calculated offline. In case of an active voltage constraint (4) an overlaying field weakening controller reduces the current reference in the d-direction such that the current reference $x_{\mathrm{ref,d}}$ is moved into the set of reachable steady states (red ellipse in Figure 2). The current reference in the q-direction $x_{\mathrm{ref,q}}$ is calculated from Equation (2) with desired torque τ_Des and d-axis current x_d replaced by their reference values. This concept is inspired by (Schröder, 2015) and depicted in Figure 4. The field weakening controller is displayed in blue. For the sake of clarity, current constraints are not considered.

2.5 Classical FOC

This section presents a classical FOC with two PI-controllers for x_d and x_q, respectively. The PI-controller feedback policy is described in the following Equation,

$$u_{\mathrm{PI},l} = k_{\mathrm{P},l} e_l(t) + k_{\mathrm{I},l} \int_0^t e_l(t)dt, \quad l \in \{d,q\}, \quad (8)$$

with the voltage $u_{\mathrm{PI},l}, l \in \{\mathrm{d},\mathrm{q}\}$ as output and error $e_l(t) = (x_{\mathrm{ref},l} - x_l), l \in \{\mathrm{d},\mathrm{q}\}$ as input. The electrical rotor speed ω is treated as a time varying parameter. For brevity, anti-wind up is not described here. Feedback decoupling is used to compensate the coupling between x_d and x_q in (1):

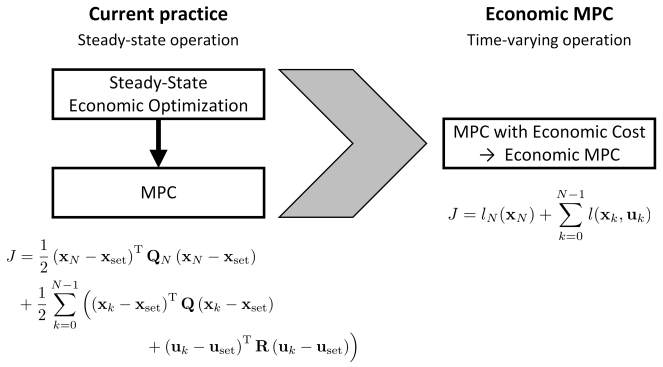

Fig. 5. Classical MPC in comparison to an economic MPC (see (Tran et al., 2014)).

$$u_{\mathrm{d}} = u_{\mathrm{PI,d}} - \underbrace{L_{\mathrm{q}}\omega x_{\mathrm{q}}}_{\text{decoupling of } x_{\mathrm{q}}}, \tag{9a}$$

$$u_{\mathrm{q}} = u_{\mathrm{PI,q}} + \underbrace{\omega(L_{\mathrm{d}}x_{\mathrm{d}} + \psi_{\mathrm{pm}})}_{\text{decoupling of } x_{\mathrm{d}} \text{ and the constant part}}. \tag{9b}$$

This results in two decoupled first order ODEs for x_{d} and x_{q} with controller voltage $u_{\mathrm{PI,d}}$ and $u_{\mathrm{PI,q}}$ as input.

$$\dot{x}_l = -\frac{R}{L_l}x_{\mathrm{l}} + u_{\mathrm{PI},l}, \quad l \in \{d, q\}. \tag{10}$$

Note that, in case of a parameter mismatch, the system is not fully decoupled, which has negative impacts on the performance and stability cannot be easily guaranteed (Schröder, 2015; Quang and Dittrich, 2008).

3. PROPOSED MPC DESIGN

In this section, first, standard concepts on classical model predictive control and economic model predictive control are briefly reviewed and then a novel field oriented economic model predictive control (FO-EMPC) formulation is presented. Especially in the field of MPC for electric motors, two main approaches are reported in the literature. In the first approach a finite control set is used, i.e. the controller output can only have a finite number of values, namely the eight inverter states (Riar et al., 2015). The second approach uses a continuous control set. In this case, the controller outputs are the line voltages, which are generated by pulse width modulation (PWM). Hence, the control is $\mathbf{u} \in \mathcal{U}$ with $\mathcal{U} \subset \mathbb{R}^{n_{\mathrm{u}}}$, where n_{u} is the dimension of the control inputs. Throughout the paper, a continuous control set based on the presented *dq*-coordinates is used.

3.1 Comparison between Classical Model Predictive Control and Economic Model Predictive Control

In the current practice, classical MPC with least squares cost is widely used. Desired set points $\mathbf{x}_{\text{set}}$ and $\mathbf{u}_{\text{set}}$ are determined by a target selector using steady state economic optimization. These set points are included in the optimal control problem (OCP) and the cost function is zero at the desired set point and positive elsewhere. The cost function in the FO-EMPC does not consider a set point and is not necessarily zero at the steady state. Therefore, a target selector or a precomputed lookup table is not necessary anymore. Figure 5 depicts classical MPC in comparison to economic MPC. Figure 6 gives an overview and depicts the related cost functions.

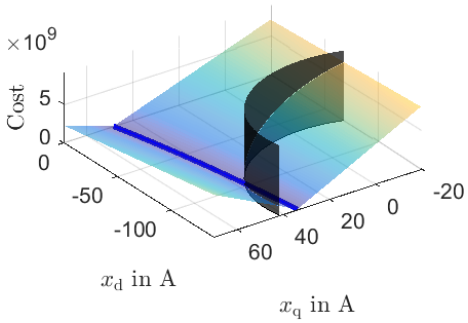

Fig. 6. Stage cost $l(\mathbf{x}_{\mathrm{k}}, s_{\mathrm{k}})$ (11a) with terminal constraints (11g) in black and 5 Nm iso torque line in blue.

3.2 FO-EMPC approach for PMSMs

The proposed FO-EMPC is based on a discrete time formulation, which are presented in Section 2. The stage cost is $l(\mathbf{x}_k, s_k) = \mathbf{x}_k^\top \mathbf{Q}\mathbf{x}_k + ws_k$ and respective for the terminal costs $l_N(\mathbf{x}_N, s_N)$. Where s_k is the L_1-slack variable at stage k and w is the weight of the slack variable. The L_1-penalty s_k enforces the desired torque τ_{Des} and due to the cost term $\mathbf{x}_k^\top \mathbf{Q}\mathbf{x}_k$ the desired torque is enforced at minimum phase currents.
The resulting optimal control problem (OCP) reads:

$$\underset{\mathbf{U},\mathbf{X},\mathbf{s}}{\text{minimize}} \quad \beta l(\mathbf{x}_N, s_N) + \sum_{k=1}^{N-1} l(\mathbf{x}_k, s_k) \tag{11a}$$

subject to

$$\mathbf{x}_{k+1} = \mathbf{A}_{\mathrm{d}}\mathbf{x}_k + \mathbf{B}_{\mathrm{d}}\mathbf{u}_k + \mathbf{f}_{\mathrm{d}}, \quad k = 0, ..., N-1, \tag{11b}$$

$$0 = \mathbf{x}_0 - \mathbf{x}(0), \tag{11c}$$

$$-s_k \leq \tau_{\mathrm{Des}} - \tau(\mathbf{x}_k) \leq s_k, \quad k = 1, ..., N, \tag{11d}$$

$$\mathbf{u}_k^\top \mathbf{u}_k \leq \frac{1}{3}U_{\max}^2, \quad k = 0, ..., N-1, \tag{11e}$$

$$\mathbf{x}_k^\top \mathbf{x}_k \leq X_{\max}^2, \quad k = 1, ..., N, \tag{11f}$$

$$(\mathbf{B}^{-1}(\mathbf{A}\mathbf{x}_N + \mathbf{f}))^\top (\mathbf{B}^{-1}(\mathbf{A}\mathbf{x}_N + \mathbf{f})) \leq \frac{1}{3}U_{\max}^2. \tag{11g}$$

Here, $\mathbf{s} = \begin{bmatrix} s_0^\top & ... & s_N^\top \end{bmatrix}^\top$ represents the slack variable sequence. The electrical rotor speed ω is regarded as a parameter. The torque $\tau(\mathbf{x}_k)$ is not measured and is calculated according to Equation (2). In Equation (11a) the controls $\mathbf{u}_k$ are not weighted, which leads to a high bandwidth and a fast control performance. In case of too high noise amplification, the bandwidth can be reduced by weighting the controller gradients $\Delta\mathbf{u}_k = \mathbf{u}_{k+1} - \mathbf{u}_k$. The matrices $\mathbf{A}_{\mathrm{d}}$, $\mathbf{B}_{\mathrm{d}}$ and the vector $\mathbf{f}_{\mathrm{d}}$ in (11b) define a discrete time representation of the *dq*-system (1). The ODE is discretized with Heun's method and rewritten in an explicit matrix equation, which depends on ω. Consequently, the discrete time description of the *dq*-system is given by:

Table 2. MPC parameter for `CasADi` and `acados`

Parameter	Value (CasADi)	Value (acados)	Unit
$\mathbf{Q}$	$\begin{bmatrix} 1 & 0 \\ 0 & 1 \end{bmatrix}$	$\begin{bmatrix} 10^{-3} & 0 \\ 0 & 10^{-3} \end{bmatrix}$	A^{-2}
w	10^9	10^3	Nm^{-1}
β	100	1	-
$U_{\max}$	48	48	V
τ_{Des}	5	5	Nm
ω	4000	4000	s^{-1}
T_{Horizon}	$250 \cdot 10^{-6}$	$500 \cdot 10^{-6}$	s
T_{s}	$125 \cdot 10^{-6}$	$250 \cdot 10^{-6}$	s
N	2	1	-

$$\mathbf{x}_{k+1} = \mathbf{A}_{\mathrm{d}}(\omega)\mathbf{x}_k + \mathbf{B}_{\mathrm{d}}(\omega)\mathbf{u}_k + \mathbf{f}_{\mathrm{d}}(\omega), \tag{12}$$

$$\text{with} \quad \mathbf{A}_{\mathrm{d}}(\omega) = \mathbf{I} + T_{\mathrm{s}}\left(\mathbf{I} + \frac{T_{\mathrm{s}}}{2}\mathbf{A}(\omega)\right)\mathbf{A}(\omega),$$

$$\mathbf{B}_{\mathrm{d}}(\omega) = T_{\mathrm{s}}\left(\mathbf{I} + \frac{T_{\mathrm{s}}}{2}\mathbf{A}(\omega)\right)\mathbf{B},$$

$$\mathbf{f}_{\mathrm{d}}(\omega) = T_{\mathrm{s}}\left(\mathbf{I} + \frac{T_{\mathrm{s}}}{2}\mathbf{A}(\omega)\right)\mathbf{f}(\omega).$$

Note that in (11d) the torque difference $\tau_{\mathrm{Des}} - \tau(\mathbf{x})$ is penalized with an L_1-penalty $|\tau_{\mathrm{Des}} - \tau(\mathbf{x})|$ instead of a quadratic term $(\tau_{\mathrm{Des}} - \tau(\mathbf{x}))^2$. The gradient of $(\tau_{\mathrm{Des}} - \tau(\mathbf{x}))^2$ is small around τ_{Des}, which would result in a significant torque offset. Theoretically, there is also a torque offset with the L_1-penalty. However, with a proper choice of the weights it is negligibly small in real situations. The term $\mathbf{x}^\top\mathbf{Q}\mathbf{x}$, which is part of the objective function, is quite different from an FO-MPC formulation, e.g. (Englert and Graichen, 2018) and (Kisner and Konigorski, 2018), due to the omitted set points, see Figure 5. Furthermore, the OCP is nonconvex due to the non-linearity introduced by $\tau(\mathbf{x})$. Only a short prediction horizon can be used due to limited computation power available in embedded systems. However, a short horizon can cause convergence and stability problems. These issues can be mitigated with an appropriate terminal weight β in Equation (11a) and a terminal set based on the time continuous system description (11g). This approach is in the spirit of (Fagiano and Teel, 2012) and, in particular the terminal set is equal to the set of reachable steady states as shown in Equation (6). The objective function and terminal set is illustrated in Figure 6. The parameters are given in Table 2. The iso-torque line for $\tau_{\mathrm{Des}} = 5$ Nm is displayed in blue, the boarder of the terminal set is represented in black.

4. SIMULATION

The performance of the proposed FO-EMPC is illustrated and a comparison between the FO-EMPC and the CFOC is shown in this section. Table 2 lists the optimization parameters, which are tailored to the specific numerical algorithms used in the paper. The software package `CasADi` is used with IPOPT, (Wächter and Biegler, 2006), as a nonlinear program solver with an exact Hessian matrix for simulation on a personal computer (Intel XEON E3-1505M v5). On dSPACE, the software package `acados` with HPIPM is used, (Frison, 2017) in combination with an SCQP scheme.

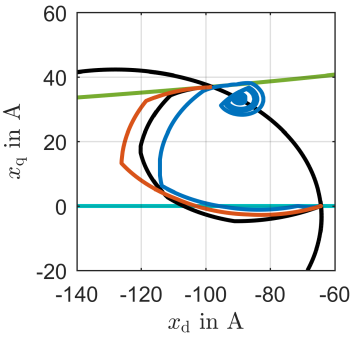

Fig. 7. The trajectories in the dq-space for three different formulation $a) - c)$. $a)$: In red the optimization problem according to (11). $b)$: In blue without terminal set (11g) and $c)$: in black with $\beta = 1$, horizon $N = 200$ and without terminal set. In cyan the 0 Nm and in green the 5 Nm iso-torque line. The boundaries of the set of steady states at $\omega = 4000\ s^{-1}$ are displayed in black.

4.1 Result of the proposed FO-EMPC formulation

In this section, a comparison between three different formulations $a) - c)$ is shown. Figure 7 shows the dq-plane with the terminal set (11g) in the interior of the black solid ellipse. The 0 Nm and 5 Nm iso-torque lines are displayed in cyan and green. The associated torque time series is displayed in Figure 8. In this test case, the electrical rotor speed is constant at $\omega = 4000\ s^{-1}$ and the desired torque rises from 0 Nm to 5 Nm. $a)$: The red solid line shows the trajectory according to optimization problem (11) with terminal cost weight $\beta = 100$. The trajectory reaches the desired torque level and the terminal set and, at the same time, the terminal penalty leads to convergence of the states to a steady state. $b)$: The blue trajectory is obtained with the same optimization problem as before, without terminal set (11g). In this case, the trajectory does not reach the desired torque and the state does not converge to a steady state. $c)$: According to problem (11a), with a horizon $N = 200$, $\beta = 1$ and without terminal set, the black solid line shows the resulting trajectory. Due to the long horizon, the states converge to a steady state, but the computation effort is much higher than with the proposed optimal control formulation. Furthermore, it is shown with a long horizon in case $c)$ only a slightly shorter transition time is obtained in comparison to case $a)$.

4.2 Comparison CFOC with FO-EMPC

In this section, a comparison between FO-EMPC and FOC is presented. In the simulation study, the desired torque is 5 Nm at a constant speed $\omega = 4000\ s^{-1}$. In Figure 9, the red solid line shows the torque step response of the FO-EMPC and the blue solid line of FOC. The desired torque rises from 0 Nm to 5 Nm and is depicted in green. As shown in Figure 10, the current trajectory of the FOC close to the boundary of the set of reachable steady states (black ellipse) and therefore the FOC needs to overcome a higher BEMF. The optimized trajectory of the FO-EMPC goes through the interior of the black ellipse, where the BEMF has a lower impact, as discussed in detail in Section 2.3. Regardless of the different trajectories, the same steady

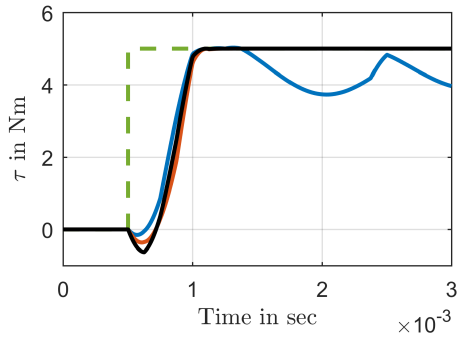

Fig. 8. The time series for three different formulations $a)-c)$. $a)$: In red the optimization problem according to (11) with respect to Table 2. $b)$: In blue without terminal set (11g) and $c)$: in black with $\beta = 1$, horizon $N = 200$ and without terminal set. The desired torque is displayed with a green dotted line.

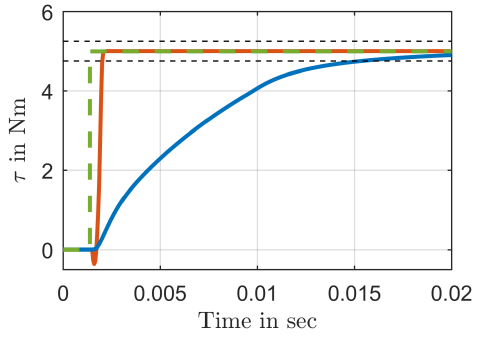

Fig. 9. The time series of the step response from 0 Nm to 5 Nm. MPC response in red and FOC response in blue. The desired torque is displayed with a green dotted line.

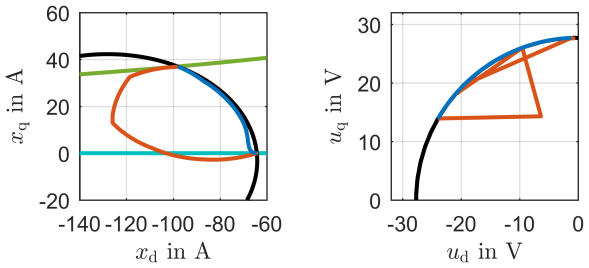

Fig. 10. Left: The trajectory of the step response in the dq-plane from 0 Nm (solid cyan line) to 5 Nm (solid green line). The trajectory of the FO-EMPC is displayed in red and in blue from the FOC. The desired torque is displayed as green dotted line. Right: The associated voltage sequence in the dq-coordinate system from the FO-EMPC in red and the FOC in blue. The circular voltage constraint is shown in black (4).

state is reached with both approaches. On the right side of Figure 10, the voltage trajectories obtained with FO-EMPC and FOC are depicted. Neither the FO-EMPC nor the FOC violate the voltage constraints.

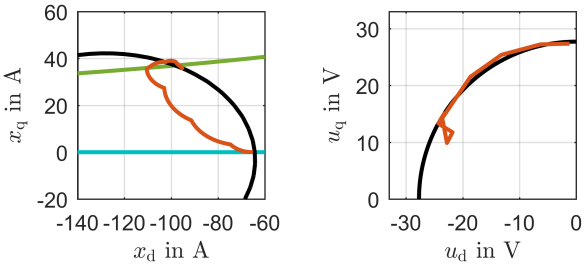

Fig. 11. Left: Step response in the dq-plane from 0 Nm (solid cyan line) to 5 Nm (solid green line) on dSPACE. The trajectory obtained with the proposed FO-EMPC is displayed in red and the desired torque as green dotted line. Right: In red the associated voltage sequence in the dq-coordinate system from the proposed FO-EMPC on dSPACE. The circular voltage constraint (4) is shown in black.

4.3 Hardware-in-the-loop (HIL) simulation

In this section, a HIL simulation of the proposed FO-EMPC is presented. The FO-EMPC is deployed on the rapid prototyping system dSPACE. In order to meet the challenging sampling time, typically required to control an electrical motor, the high performance software package `acados` (Verschueren et al., 2019) with the solver HPIPM is used which targets MPC applications as this one. A sequential convex quadratic programming scheme (SCQP) is used (Verschueren et al., 2016) in order to exploit convexity of the quadratic constraints (11e) and (11g) obtain a better Hessian approximation. Furthermore, in order to reduce the computational effort, a real-time iteration (RTI) scheme, (see (Diehl et al., 2005)), is used based on quadratic subproblems. Due to the fact that the RTI exploits solutions to QPs that locally approximate (11), only linear constraints can be satisfied exactly. On the contrary, nonlinear constraints, such as (11e), are only satisfied "in the limit", as the system state converges to a steady state. As the sampling time is chosen relatively high a multiple shooting method with an implicit Runge Kutta first order method ($IRK1$) is used, due to the larger stability region in comparison to explicit methods. In Figure 11, the closed-loop behaviour obtained with a desired torque step from 0 Nm to 5 Nm together with the associated control sequence are shown. On the left side, the resulting current trajectory is shown. The trajectory is similar to the simulated trajectory in `CasADi` from Section 4.2, but closer to the boundaries (black ellipse) than the simulated one with `CasADi`. The steady state at the end is different, too, which results in a small torque offset (see Figure 12). The different behaviour between `acados` and `CasADi` is caused by the already mentioned methods in order to reduce the computation time. On the right side of Figure 11 the associated control trajectory is depicted. The circular voltage constraints (black solid line) are not satisfied in every time step, due to the inexactness introduced by the RTI scheme. In Figure 12 a comparison is given between FOC from Section 4.2 and the real-time implementation of FO-EMPC. The computation time on dSPACE DS1007 is shown in Figure 13, which is between 137 and 225 μs and hence less than the required sample time $T_s = 250$ μs displayed as red solid line in Figure 13.

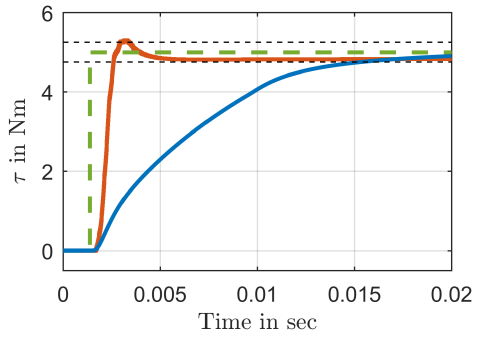

Fig. 12. Step response from 0 Nm to 5 Nm on dSPACE. The FO-EMPC response is figured in red. The desired torque is displayed as green dotted line. The blue solid line is the torque response of the FOC from Section 4.2.

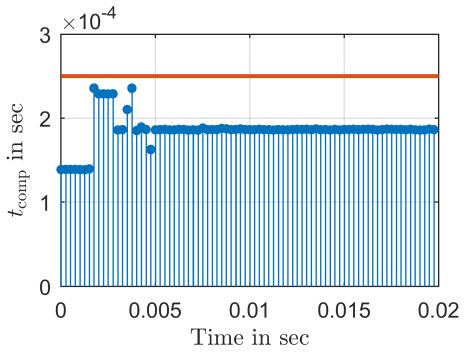

Fig. 13. The computation times on dSPACE associated with Figure 11 and 12. The red solid line shows the nominal sample time $T_s = 250\ \mu s$.

In the HIL simulation the current constraints (11f) are neglected, because the current constraint is always inactive at speed $\omega = 4000\ s^{-1}$.

5. CONCLUSIONS AND OUTLOOK

This paper presents an economic model predictive torque control which uses the set of steady states as terminal set in order to drastically reduce the prediction horizon and hence improve the computation times. It is shown that the performance is significantly better in comparison to classical FOC, leading to a settling time 25 times shorter than FOC. The proposed approach allows a compact and flexible formulation without precomputed set points. Further research will target the combination of the proposed approach with a high gain observer to reach offset free control and the consideration of current-dependency of the inductance in the FO-EMPC. Furthermore, the FO-EMPC will be tested with the the rapid prototyping system dSPACE using the software package `acados` (Verschueren et al., 2019) on test bench in order to analyse its behaviour on real experiments.

REFERENCES

Andersson, J.A.E., Gillis, J., Horn, G., Rawlings, J.B., and Diehl, M. (2018). CasADi: a software framework for nonlinear optimization and optimal control. *Mathematical Programming Computation*.

Diehl, M., Bock, H., and Schlöder, J. (2005). A real-time iteration scheme for nonlinear optimization in optimal feedback control. *SIAM J. Control and Optimization*, 43, pp. 1714–1736.

Englert, T. and Graichen, K. (2018). A fixed-point iteration scheme for model predictive torque control of PMSMs. *IFAC-PapersOnLine*, 51, pp. 568–573.

Fagiano, L. and Teel, A.R. (2012). On generalized terminal state constraints for model predictive control. *CoRR*, abs/1207.0788.

Findeisen, R., Graichen, K., and Mönnigmann, M. (2018). Eingebettete Optimierung in der Regelungstechnik Grundlagen und Herausforderungen. *at - Automatisierungstechnik*, 66, pp. 877–902.

Frison, G. (2017). HPIPM, High-performance interior-point qp solvers. https://github.com/giaf/hpipm.

Graber, S. (2018). Time-optimal control of electric machines with state and input constraints.

Kisner, V. and Konigorski, U. (2018). Model predictive torque control of a synchronous reluctance machine. In *6th IFAC Conference on Nonlinear Model Predictive Control*.

Konigorski, U. (2011). *Controller Design for Multivariable Systems in State Space*. Script TU Darmstadt.

Kouzoupis, D., Frison, G., Zanelli, A., and Diehl, M. (2018). Recent advances in quadratic programming algorithms for nonlinear model predictive control. *Vietnam Journal of Mathematics*, vol. 46.

Quang, N. and Dittrich, J. (2008). *Vector Control of Three-Phase AC Machines: System Development in the Practice*. Power Systems. Springer Berlin Heidelberg.

Riar, B., Geyer, T., and Madawala, U.K. (2015). Model predictive direct current control of modular multilevel converters: Modeling, analysis, and experimental evaluation. *IEEE Transactions on Power Electronics*, 30, pp. 431–439.

Schröder, D. (2015). *Elektrische Antriebe - Regelung von Antriebssystemen*. Springer Berlin Heidelberg.

Tran, T., Ling, K., and Maciejowski, J. (2014). Economic model predictive control - a review. *31st International Symposium on Automation and Robotics in Construction and Mining, ISARC 2014 - Proceedings*.

Verschueren, R., Frison, G., Kouzoupis, D., van Duijkeren, N., Zanelli, A., Novoselnik, B., Frey, J., Albin, T., Quirynen, R., and Diehl, M. (2019). acados: a modular open-source framework for fast embedded optimal control. *arXiv*.

Verschueren, R., van Duijkeren, N., Quirynen, R., and Diehl, M. (2016). Exploiting convexity in direct optimal control: a sequential convex quadratic programming method. In *Proceedings of the IEEE Conference on Decision and Control (CDC)*.

Wächter, A. and Biegler, L.T. (2006). On the implementation of a primal-dual interior point filter line search algorithm for large-scale nonlinear programming. *Mathematical Programming 106*, (1), pp. 25–57.

Zanelli, A., Kullick, J., Eldeeb, H., Frison, G., Hackl, C., and Diehl, M. (2019). Continuous control set nonlinear model predictive control of reluctance synchronous machines. *IEEE Transactions on Control Systems Technology (accepted) - https://arxiv.org/abs/1910.10681*.